Published in final edited form as:
ACS Nano. 2019 June 25; 13(6): 7300–7309. doi:10.1021/acsnano.9b03444.

Metal-Ion Modulated Structural Transformation of Amyloid-Like Dipeptide Supramolecular Self-Assembly

Wei Ji[†,‖], **Chengqian Yuan**[‡,‖], **Shai Zilberzwige-Tal**[†], **Ruirui Xing**[‡], **Priyadarshi Chakraborty**[†], **Kai Tao**[†], **Sharon Gilead**[†], **Xuehai Yan**[*,‡], **Ehud Gazit**[*,†,§]

[†]Department of Molecular Microbiology and Biotechnology, George S. Wise Faculty of Life Sciences, Tel Aviv University, Tel Aviv 6997801, Israel

[‡]State Key Laboratory of Biochemical Engineering, Institute of Process Engineering, Chinese Academy of Sciences 100190 Beijing, China

[§]Department of Materials Science and Engineering Iby and Aladar Fleischman Faculty of Engineering Tel Aviv University, Tel Aviv 6997801, Israel

Abstract

The misfolding of proteins and peptides potentially leads to a conformation transition from an α-helix or random coil to β-sheet-rich fibril structures, which are associated with various amyloid degenerative disorders. Inhibition of the β-sheet aggregate formation and control of the structural transition could therefore attenuate the development of amyloid-associated diseases. However, the structural transitions of proteins and peptides are extraordinarily complex processes that are still not fully understood and thus challenging to manipulate. To simplify this complexity, herein, the effect of metal ions on the inhibition of amyloid-like β-sheet dipeptide self-assembly is investigated. By changing the type and ratio of the metal ion/dipeptide mixture, structural transformation is achieved from a β-sheet to a superhelix or random coil, as confirmed by experimental results and computational studies. Furthermore, the obtained supramolecular metallogel exhibits excellent *in vitro* DNA binding and diffusion capability due to the positive charge of the metal/dipeptide complex. This work may facilitate the understanding of the role of metal ions in inhibiting amyloid formation and broaden the future applications of supramolecular metallogels in three-dimensional (3D) DNA biochip, cell culture, and drug delivery.

Author Contributions

[‖]W.J. and C.Y. contributed equally. W.J., C.Y., X.Y., and E.G. conceived and designed the work. W.J., K.T., and S.G. conducted gelation, TEM, FTIR, and CD characterizations. W J. and P.C. conducted measurements of fluorescent emission and rheology properties for gels. C.Y. and R.X. performed AFM images and DFT calculations. S.Z.-T. conducted the DNA binding assays. W.J., C.Y., X.Y., and E.G. cowrote and edited the manuscript. All authors discussed and commented on the manuscript.

[*]**corresponding authors**: yanxh@ipe.ac.cn; ehudg@post.tau.ac.il.

The authors declare no competing financial interest.

Europe PMC Funders Author Manuscripts

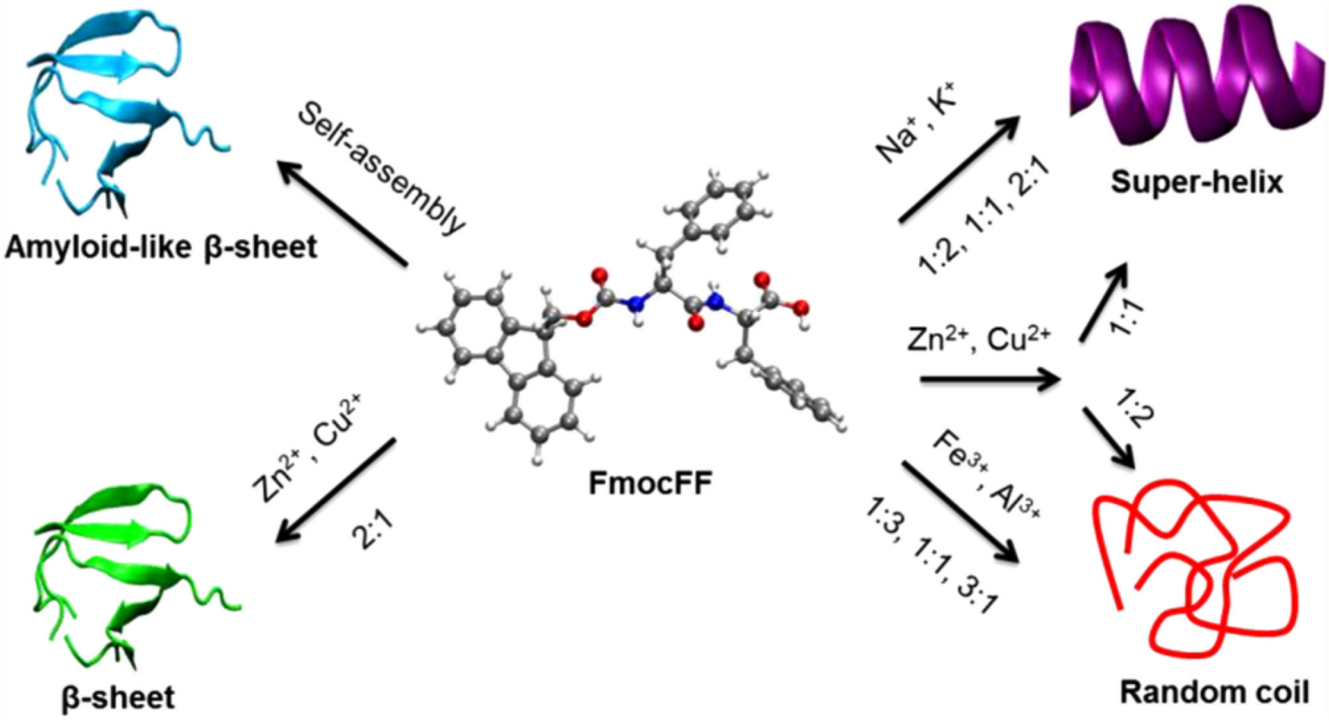

Keywords

hydrogels; self-assembly; nanostructures; dipeptide; supramolecular chemistry

The aggregation of proteins and peptides into amyloid fibrils has attracted a considerable amount of attention in the fields of structural biology, medicine, chemistry, physics, and materials science,[1–4] since it is a ubiquitous phenomenon associated with neurodegenerative disorders such as Alzheimer's, Parkinson's, and Huntington's diseases.[5–11] Under the influence of modified conditions, these proteins and peptides may partially unfold and subsequently assemble into insoluble, highly ordered antiparallel β-sheet rich fibrous structures.[12,13] Both random coil to β-sheet and helix to β-sheet transitions could occur during the misfolding process, inducing amyloid diseases.[14] Although the pathogenesis of these diseases has been established to be associated with the process of amyloid formation, the mechanism of structural transitions associated with protein and peptide misfolding remains unclear. Thus, regulation of the structural transformation of the stable and highly ordered β-sheet conformation into the helix or random coil bears important implications for inhibiting amyloid fibril formation and still remains an urgent unmet challenge.

Due to the moderate bond strength and reversibility, supramolecular interactions of misfolded proteins and peptides are usually formed in response to different physical and chemical stimuli (e.g., temperature,[15,16] Coulomb interaction,[17] pH,[18,19] metal ions,[20,21] and chemical additives[22,23]), which induce structural transformation. Among these stimuli, metal ions, mainly copper, zinc, and iron, have been proposed to play a key role in several processes associated with the etiology of Alzheimer disease, but their role is not yet fully

Europe PMC Funders Author Manuscripts

understood.[24] Depending on the position of coordination residues, metal-ion complexation was shown to either inhibit or accelerate the amyloid formation process through rational control of noncovalent interactions,[25–37] such as metal coordination, hydrogen bonding, and π–π stacking, further inducing rearrangement of the protein main chain and determining the major secondary structures. To the best of our knowledge, the disruption of β-sheet formation and further structural transition into a helix or random coil triggered by changing the type and stoichiometry of metal ions has been rarely reported, and no genuine understanding of the mechanism of structural modification is available.

To simplify the complexity of proteins and peptides, we chose a reductionist approach aimed at understanding the fundamental role of metal ions in the formation of amyloids by a short peptide model. The diphenylalanine (FF) peptide was identified as the smallest unit and the core recognition motif of the Alzheimer's β-amyloid polypeptide that can self-assemble into tubular structures with the characteristic amyloid-like structural signatures, rather than into fibrous structures.[38–43] Following modification by aromatic protection of FF, the extensively studied 9-fluorenylmethoxycarbonyl (Fmoc)-modified dipeptide (FmocFF) self-assembles into highly ordered antiparallel β-sheet rich typical amyloid-like fibrils through hydrogen bonding and π–π stacking.[44–50] Regarding the strong coordination interactions between carbonyl groups and metal ions, the regulation of the structural transition of FmocFF self-assembly may be modulated by changing the type and ratio of metal ions. Herein, a facile route is developed to explore the effect of metal ions on the structural transformation of amyloid-like β-sheet self-assembled FmocFF into superhelix or random coil conformations. The metal coordination is shown to lead to a structural transition of the supramolecular β-sheet self-assembly with varying different valences of metal ions and ratios of metal ions/ dipeptide (Figure 1). The secondary structures and morphologies of the metal ion/ dipeptide assemblies are fully investigated by circular dichroism (CD), Fourier transform infrared (FTIR), transmission electron microscopy (TEM), and atomic force microscopy (AFM). The proposed models for metal ions-peptide coordination are further confirmed by density functional theory (DFT) calculations. Moreover, the introduction of metal ions coordination into peptide assembly typically endows the nanofibrils with a positive charge, which improves the DNA binding ability of the FmocFF-based supramolecular metallohydrogels. This study may facilitate the understanding of the role of metal ions in inhibiting amyloid formation and broaden the future applications of the supramolecular metallogels in 3D DNA biochips and cell culture.

Results and Discussion

Based on the different coordination properties of metal ions, we chose metal ions of different valences for this study (Na^+, K^+, Zn^{2+}, Cu^{2+}, Fe^{3+}, Al^{3+}). The dynamic gelation behaviors of FmocFF in the presence of different ratios of the various metal ions were investigated by recording time lapse optical images. All of the metal ion solutions are transparent before addition of FmocFF dipeptide. At a concentration of 2.0 mg/mL, single-component FmocFF formed a self-supported and invertible gel in 2% DMSO in H_2O (v/v) (Figure 2a). The inverted test tube method indicated that following the addition of FmocFF to most of the monovalent and divalent metal ion solutions at different molar ratios, ranging from 2:1 to 1:2, hydrogels were formed, except for FmocFF/Cu^{2+} (1:2) (Figure 2a and Figures S1

and S2). However, no gel was formed except for a precipitate in the presence of trivalent metals at different molar ratios, ranging from 3:1 to 1:3 (Figure 2a and Figure S3). It also should be noted that the time required for the transition from the opaque emulsion of FmocFF to relatively transparent gels was substantially different in the presence of the different metal ions, varying from ~5 min for single FmocFF, ~8 min for FmocFF/Na^+ and FmocFF/K^+, to ~30 min for FmocFF/ Zn^{2+} and FmocFF/Cu^{2+}. No transparency transition was observed for FmocFF/Fe^{3+} and FmocFF/Al^{3+}. These findings indicated the different assembly behaviors of FmocFF in the presence of various metal ions. To quantify the kinetics of the assembly process, we monitored the time-dependent absorbance of the metal/dipeptide solutions at 405 nm for transparency change (Figure 2b). The absorbance of single FmocFF solution started to decrease after 282 s and reached an optical density (OD) of 0.18 after 1460 s, while the absorbance in the presence of metal ions solution reached different OD values depending on the valence of the metal ion (Figure S4). For the monovalent metal ions, the OD value reached approximately 0.5 after 1800–3600 s, and an OD value of ~1.5 was obtained after 2400 and 8000 s in the presence of Zn^{2+} and Cu^{2+} divalent ions, respectively. The OD value remained around 3.5 throughout the experiment for Fe^{3+} and Al^{3+}. The kinetics of fiber formation by the FmocFF/metal ions solution was slower than that of FmocFF, indicating that metal coordination interactions indeed occurred, possibly regulated by the different molar ratio of the two components. It should be noted that there was a difference between the time frames of the vial turbidity assay and the absorbance measurement at 405 nm, possibly due to the different solution volumes used in each experiment, which affected the assembly kinetics.

We next aimed to measure the mechanical rigidity of the different metal-incorporated peptide-based hydrogels using rheology. We first performed the strain sweep experiment to determine the linear viscoelastic regime, followed by a frequency sweep experiment to confirm the formation of gels. Rheological studies of pure FmocFF hydrogel exhibited a breakage strain of 52%, along with a frequency-independent nature of the storage (G′) and loss (G′′) moduli, a characteristic signature of gelation[51] (Figure S5). Subsequently, we analyzed the rheological properties of the corresponding metallohydrogels (Figure S6). The strain sweep experiments carried out on the metallohydrogels composed of monovalent ions revealed almost identical results compared to the pure Fmoc-FF hydrogel for each molar ratio. However, for the divalent metal ions, the breakage strain increased in most cases (except for 1:1 FmocFF/Cu^{2+}), reached above 100%, and was accompanied by a decrease in the modulus values. Lower moduli indicate less rigid fibers capable of withstanding higher values of shear resulting in increased breakage strain. On the other hand, stiff gels break at lesser strain values, as they are composed of a network of less elastic, rigid fibers. Therefore, the metallogels comprising divalent metal ions break at higher strain values compared to single FmocFF and the monovalent counterparts. Frequency sweep experiments on the metallogels (Figure 2c and Figure S7) showed an increase in the G′ value for low concentrations of the monovalent metal ions (2:1 FmocFF/Na^+ and FmocFF/ K^+) indicating stiffer gel formation, probably indicating the increased number of supramolecular interactions due to the coordination of metal ions and FmocFF. However, the G′ decreased with further increase in Na^+/K^+ concentration (1:1 and 1:2 FmocFF/Na^+ and FmocFF/K^+), indicating weaker network formation after addition of excess metal ions. For the divalent

metal ions, a drastic decrease of both G′ and G′′ was observed for all the gels, which may be ascribed to the stronger metal ion/FmocFF coordination. The G′′ value was higher than G′ for FmocFF/Cu^{2+} (1:2) due to no self-supported gel formation under these conditions. Notably, rheological properties of FmocFF/trivalent ions were not evaluated as these hybrids failed to form gels.

The microstructures of FmocFF and FmocFF/metal ions were investigated by TEM and AFM, allowing us to examine the size and height distribution of the assemblies. Single FmocFF formed well-defined entangled nanofibrous structures ~8 nm in average diameter and ~5–10 nm in height (Figure 2d,h). However, improved average size distribution of 10–20 nm in diameter was observed following the addition of monovalent or divalent metal ions at different ratios (Figure 2e,f and Figures S8 and S9), with the largest size distribution of nanofibrils observed for FmocFF/Cu^{2+}. In the presence of the trivalent metal ions, the FmocFF/metal complex generated spherical structures with a maximal size of 90–100 and 50–70 nm for Fe^{3+} and Al^{3+}, respectively (Figure 2g and Figure S10). It should be ascribed to the enhanced hydrophobic interactions induced by the relative strong binding between dipeptides and metal ions, which inhibit the further assembly of spheres into nanofibrils.[52] The morphologies of FmocFF/ metal ions, as observed by AFM images, were in good agreement with the results of the TEM analysis, with height distributions of 5–15 and 5–40 nm for mono-/divalent and trivalent metal ions, respectively (Figure 1i–k and Figure S11). These results suggest the self-assembly of FmocFF is influenced by the metal/dipeptide coordination interactions.

To investigate the effect of metal ions on the secondary structure of amyloid-like dipeptide self-assembly, CD spectra of metal ion/dipeptide assemblies in the far UV region of 190–260 nm were recorded. For FmocFF self-assembled in the absence of metal ions (Figure 3a), positive and negative Cotton effects were observed at 194 and 218 nm, respectively, indicating a β-sheet rich structure. When examining different ratios of FmocFF/Na^{+} and FmocFF/K^{+}, an α-helix-like CD pattern comprising one maximum positive peak at 192–194 nm and two minimum negative peaks at 203–205 and 214–216 nm were observed for all of the assemblies (Figure 3b,c and Figure S12a–d), suggesting a structural transition from β-sheet into superhelix-rich conformations. The CD spectra for FmocFF/monovalent metal ions showed blue-shifted α-helixlike patterns in its minima, compared to that of canonical longer α-helical peptides (208 nm, 222 nm), as previously observed and defined as characteristic of helical conformations of short peptide.[53,54] Our group has also reported a self-assembling single heptad repeat module to form a superhelical conformation, where the peptide exhibited two negative maxima at around 205 and 218 nm.[55] Thus, the helical conformation of metal ion/dipeptide should be ascribed to the type of superhelix stabilized by metal coordination and intermolecular noncovalent interactions. For the divalent metal ions, the structural conformations were strongly related to the ratio of metal ion/dipeptide. After coordination with Zn^{2+}/Cu^{2+} at a ratio of 2:1 (Figure 3d and Figure S12i), one maximum peak at 194 nm and one minimum peak at 205 nm were obtained, demonstrating a blue shift (13 nm) of the minimum peak, thus indicating highly ordered β-sheet-rich assemblies. However, one maximum positive peak at 192 and two minimum negative peaks at 202 and 208 nm were observed by changing the ratio of FmocFF/Zn^{2+} to 1:1, suggesting a superhelix rich conformation in the assemblies (Figure 3i). Interestingly, the FmocFF/Cu^{2+}

(1:1) assembly showed two minimum peaks identical to those of the canonical longer α-helical peptides (208, 222 nm), possibly indicating a very similar helical structural conformation (Figure S12j). β-Sheet- and α-helix-like CD patterns were completely absent for the FmocFF/Zn^{2+} (1:2) and FmocFF/Cu^{2+} (1:2) assemblies. Similar random coils were found for FmocFF in the presence of trivalent metal ions at different ratios (Figure 3j–l and Figure S12k,l,q–s).

High-resolution TEM images were investigated to study the nanostructures formed by metal ion/FmocFF following secondary structural transition by metal coordination. Relatively flat fibrils were observed for all β-sheet-rich assemblies formed by FmocFF, FmocFF/Zn^{2+} (2:1), and FmocFF/Cu^{2+} (2:1) (Figure 3e,h and Figure S12m). However, right-handed helical fibrils were observed for the superhelix rich samples of FmocFF/Na^{+} (2:1, 1:1, 1:2), FmocFF/K^{+} (2:1, 1:1, 1:2), FmocFF/Zn^{2+} (1:1), and FmocFF/Cu^{2+} (1:1) (Figure 3f,g,m and Figure S12e–h,n), revealing extensive fiber network formation with helical substructures. For the random coil substructures formed by FmocFF/Zn^{2+} (1:2), FmocFF/Cu^{2+} (1:2), FmocFF/Fe^{3+} (3:1, 1:1, 1:3), and FmocFF/Al^{3+} (3:1, 1:1, 1:3), both nanofibrils and spheres were found (Figure 3n–p and Figure S12o–p,t–v). Random coils based assemblies by FmocFF/Zn^{2+} (1:2) and FmocFF/Cu^{2+} (1:2) are nontypical fibrous structures. Such nonamyloid nanofibrils have also been reported in the self-assembly of ovalbumin, which does not only form amyloid fibrils but also nonamyloid fibrils at low pH conditions.[56]

In order to further explore the underlying mechanism of metal coordination induced structural transition of amyloidlike dipeptide self-assembly, the formation of a β-sheet by single FmocFF and FmocFF/Zn^{2+} (2:1) and of superhelix by FmocFF/Na^{+} (1:1) and FmocFF/Zn^{2+} (1:1) was studied by FTIR spectroscopy, fluorescence emission, and DFT calculations. Changes in the solid state of characteristic FTIR absorption peaks could reflect the interaction of metal ions with the possible binding sites of amide/carbonyl groups in the FmocFF dipeptide. The 3500–3200 cm^{-1} region representing amide A bands is important for assessing N–H stretching vibrations, providing information on hydrogen-bonding interactions. The 1800–1500 cm^{-1} region corresponds to the stretching band of amide I and the bending peak of amide II (Figure 4a). The FTIR spectrum of FmocFF showed amide A bands at 3304 and 3448 cm^{-1}, indicating that free N–H and intermolecular hydrogen-bonded N–H, respectively. The amide I and amide II bands appeared at 1746, 1692, 1661, 1605, and 1536 cm^{-1}. In FmocFF/Na^{+} (1:1), the amide A bands at 3448 cm^{-1} split into two peaks of 3474 and 3414 cm^{-1}, indicating different intermolecular hydrogen bonding interactions between amide groups in the assembly. This hydrogen bonding was also weakened in the presence of Zn^{2+} for both the 2:1 and 1:1 ratios since the peak at 3448 cm^{-1} became weaker by increasing the concentration of Zn^{2+}. The amide I and amide II bands of the metallogels appeared at FmocFF/Na^{+} (1:1) (1746, 1692, 1656, 1535 cm^{-1}), FmocFF/ Zn^{2+} (2:1) (1696, 1662, 1538), and FmocFF/Zn^{2+} (1:1) (1694, 1654, 1534 cm^{-1}). The stretching vibration band of C═O from carboxyl groups at 1746 cm^{-1} became weak for FmocFF/Na^{+} (1:1) and almost disappeared for FmocFF/Zn^{2+} (2:1) and FmocFF/ Zn^{2+} (1:1), suggesting a better coordination ability of Zn^{2+} with the carbonyl groups, as compared to Na^{+}.[20] Furthermore, for FmocFF/Na^{+} (1:1) and FmocFF/ Zn^{2+} (1:1), the intense bands at 1656 and 1654 cm^{-1}, respectively, could be ascribed to the predominantly helical conformation,[57] in good agreement with the CD spectra analysis.

A fluorescence emission spectrum was employed to study the π–π interactions between aromatic groups, which play an important role in stabilizing the 3D structural conformation of the supramolecular gels. As shown in Figure 4b, compared to the maximum emission wavelength of FmocFF solution in DMSO (312 nm), red shifts were observed for all the hydrogels, indicating that π–π interactions between Fmoc groups take place during FmocFF aggregation. Compared to the maximum emission wavelength of FmocFF and FmocFF/ Na^+ (1:1) at 322 nm, a slight red shift was observed for FmocFF/Zn^{2+} (2:1) and FmocFF/Zn^{2+} (1:1) at 324 nm. Moreover, the strong fluorescence emission was observed for FmocFF/Zn^{2+}, which could be ascribed to the chelationenhanced fluorescence (CHEF) effect allowing bouncing back of an excited electron from the lowest unoccupied molecular orbital (LUMO) back to the highest occupied molecular orbital (HOMO) of the fluorophore upon the addition of Zn^{2+}.[58]

DFT calculations were further performed to unravel the possible coordination modes within the dipeptide–metal ion complexes during the self-assembly process. The stable conformation of FmocFF homoclusters is shown in Figure 4c. An antiparallel β-sheet is formed through the hydrogen bonding between amide groups and π–π stacking between aromatic groups. The optimized structure of the FmocFF/Zn^{2+} (2:1) complex is depicted in Figure 4d. The binding sites of carbonyl groups from amide and carboxylic group were identified for FmocFF/Zn^{2+} (2:1), in which Zn^{2+} can coordinate with two dipeptide molecules and influence the molecular organization of the dipeptide. In the optimized conformers of FmocFF/Na^+ (1:1) and FmocFF/Zn^{2+} (1:1), metal ions coordinate with two carbonyl oxygen atoms within the main chain of FmocFF (Figure 4e,f), which result in the conformational transformation of the dipeptide, probably inducing the formation of superhelix structures with further assembly by the metal ion/dipeptide complex. Notably, FmocFF cannot further assemble into nanofibrils instead of spheres in the presence of trivalent metal ions due to the very strong metal coordination interactions, which induce random coils. In this work, we studied the molecular coordination between metal ions and dipeptides by DFT calculations. It should be noted that the interactions between metal ion–amyloid fibrils are also interesting and have been reported at both structural and thermodynamic levels for the application of industrial water purification technologies.[59,60] The binding ability of metal ions to amyloid FmocFF fibrils will be investigated in our future work.

The above results of FTIR, fluorescence emission, and DFT calculations reveal that the self-assembly behavior of the dipeptide is influenced upon the coordination between carbonyl groups and metal ions and that the synergic effect of metal coordination, hydrogen bonds, and π–π stacking induces the structural transformation of amyloid-like dipeptide self-assemblies.

DNA biochips consisting of DNA sequences covalently bound/attached to solid substrates (e.g., glass, silicon, polymers) have gained considerable interest for the fast and efficient detection of pathogens. However, the restricted hybridization efficiency and the limited loading capacity of surface materials are the main disadvantages of two-dimensional (2D) DNA chips. As an alternative approach, supra-molecular metal–peptide hydrogels may exhibit excellent DNA binding and diffusion capability due to the 3D network, utilizing

the positive charge of the metal–peptide complex for fast binding of the negative DNA (Figure 5a and Figure S13).[61] DNA-binding assays of different metallogels mixed at various ratios indicated that Zn^{2+}-containing metallogels bound DNA faster than that gels containing Na^{+} and the control FmocFF gel. While the fluorescence of Zn^{2+}-containing metallogels decreased to below 20% after 0.5-h incubation with DNA, the fluorescent signal of Na^{+}-containing metallogels decreased much more slowly with no change for single FmocFF gel (Figure 5b). Although Na^{+}-containing metallogels and the single FmocFF gel showed a DNA binding property for a long time, the binding capacity of Zn^{2+}-containing metallogels was supposed to be higher due to more effective DNA binding within 0.5 h (Figure 5c). This could be explained by the strong ability of Zn^{2+} to bind both the negative phosphate groups in the DNA backbone and the DNA bases, while Na^{+} only binds the phosphate groups.[57] TEM images of FmocFF/Zn^{2+} (1:1) and FmocFF gels after 0.5 h incubation with DNA are shown in Figure S14. Many plasmid DNA molecules 10–50 nm in size were found to be encapsulated in the FmocFF/Zn^{2+} gel network, but not in the single FmocFF, in good agreement with the results of fluorescence assay (Figure 5b). Time-dependent TEM images of the FmocFF/Na^{+} (1:1) hydrogel with DNA solution also indicated the increasing binding of DNA molecules to the 3D gel network from 0 to 7 h. This result reveals that the supramolecular metallohydrogels may find potential application in the construction of 3D DNA biochips.

Conclusion

In summary, the metal ion-modulated structural transformation from an amyloid-like β-sheet into superhelix or random coil has been successfully achieved by changing the types and ratios of metal ion/dipeptide through metal coordination, hydrogen bonding, and π–π stacking. The structural transformation of dipeptide self-assembly regulated by metal ions is fully demonstrated by CD spectroscopy, TEM images, AFM images, FTIR spectroscopy, and DFT calculations. The in vitro DNA binding abilities of metallohydrogels are further studied by fluorescence spectroscopy and TEM images, indicating the fast binding and good loading capacity of the dipeptide/Zn^{2+} gel network. The present work not only exemplifies a feasible strategy to explore the effect of metal ions on the inhibition of amyloid-like structure formation by short dipeptide building blocks but also may lay the basis for various future applications of supramolecular metallogels, including 3D DNA biochip, cell culture, and drug delivery.

Experimental Methods

Gel Preparation

A 10 μL dimethyl sulfoxide (DMSO) solution of FmocFF was added to 490 μL double-distilled water containing different concentrations of metal ions (NaCl, KCl, $ZnCl_2$, $CuCl_2$, $FeCl_3$, $AlCl_3$) to a final gelator concentration of 2.0 mg/mL. Gel formation was evaluated by the “inverted-vial” method. All of the fresh metal ion solutions are transparent and used for the experiments. 0 min represents the starting point after addition of FmocFF into the different metal ion soultions.

Europe PMC Funders Author Manuscripts

Turbidity Assay

A 200 μL amount of only FmocFF and different ratios of FmocFF/metal ions were prepared as described above and put into a 96-well plate. Absorbance at 405 nm was measured every 10 s using a TECAN Infinite M200PRO plate reader until the equilibrium value was reached.

Rheology

Rheological studies were performed on an ARES-G2 rheometer (TA Instruments, New Castle, DE) using a 20 mm parallel-plate geometry with a gap of 1000 μm. One-day aged gels were used for the measurements. Dynamic frequency sweep experiments were carried out at a constant strain of 0.1%. Strain sweep was carried out at a constant frequency of 1 Hz.

TEM Images

Aliquots (10 μL) of diluted gel solution were added into a glow discharge copper grid (400 mesh) coated with thin carbon film for 2 min. Excess solution was then removed, and the grid was washed with deionized water three times and stained with 2.0% (w/v) uranyl acetate (UA) by exposing the grid to one drop of UA solution for 60 s. TEM images were viewed using a JEOL 1200EX electron microscope operating at 80 kV.

AFM Images

Samples of FmocFF/metal ions were deposited onto freshly cleaved mica without any dilution and dried with an air flow in a thermostatic vacuum drier. AFM scanning was conducted using a Bruker (USA) Dimension Ion operated in tapping mode with a ScanAsyst-Air cantilever under ambient conditions. The structures of interest were analyzed in the section profile using a Nano-Scope Analysis software.

FTIR Spectroscopy

A 250 μL portion of each gel was deposited onto a real crystal KBr IR card (International Crystal Laboratories, Garfield, NJ) and vacuum-dried. The dried sample was then wetted three times with 1 mL of D_2O. The FTIR spectra were recorded on a Nicolet 6700 FTIR spectrometer (Thermo Scientific, Waltham, MA), from 4000 to 400 cm^{-1} at room temperature. The background signal was recorded using D_2O and subtracted to obtain each FTIR spectrum.

CD Spectroscopy

CD spectra of all the samples were collected on a carried out with an Applied Photophysics Chirascan spectrometer with a bandwidth of 1.0 nm in the ultraviolet (UV) region (190–260 nm) using a 0.1 mm quartz cuvette. All scans were performed at a scan speed of 30 nm min^{-1} with a data pitch of 0.5 nm at room temperature. All spectra were obtained following solvent background subtraction. The reported spectra represent the average of three scans.

Computational Methods

To determine the coordination environment of the metal ion (M^{n+}) within the FmocFF-M^{n+} complex, density functional theory (DFT) calculations were carried out using the Gaussian 09 package.[62] Full geometry optimizations of the FmocFF–M^{n+} complex with different structures were carried out using the Becke three-parameter hybrid (B3LYP) exchange-correlation function without symmetry constrains.[63] The standard split-valence 6-31G(d) basis set of atomic orbitals was used for H, C, N, O, and Na atoms, and the Zn^{2+} was described by the LANL2DZ relativistic pseudopotentials.[64] Harmonic vibrational frequency calculations on the optimized geometries were also performed to ensure the structures were at local minima.

DNA Binding

The interactions between plasmid DNA (pDNA) and metallogels were detected by fluorescence measurements. pDNA (pET14b-eGFP) (7.5 μg/mL^{-1}) and SyberSafe (SS) (X10,000) were dissolved in double-distilled H_2O and incubated for 30 min at room temperature. A total of 1000 μL of the pDNA-SS solution was transferred to the wells of a black 96-well plate containing 350 μL metallogels at different dipeptide/metal ion ratios. An aliquot of 50 μL was taken at defined times and returned after fluorescence measurement (excitation wavelength at 502 nm and emission wavelength at 530 nm). A mixture containing only pDNA, SS, and double-distilled H_2O served as the calibration standard.

Supplementary Material

Refer to Web version on PubMed Central for supplementary material.

Acknowledgments

This work was supported by the European Research Council under the European Union Horizon 2020 research and innovation program (No. 694426) (E.G.) and the National Natural Science Foundation of China (Project Nos. 21522307 and 21802143), the National Natural Science Fund BRICS STI Framework Programme (No. 51861145304), Innovation Research Community Science Fund (No. 21821005), and the Key Research Program of Frontier Sciences of Chinese Academy of Sciences (CAS, Grant No. QYZDB-SSWJSC034) (X.Y.). We thank Dr. Sigal Rencus-Lazar for language editing assistance.

References

(1). Caughey B, Lansbury PT. Protofibrils, Pores, Fibrils, and Neurodegeneration: Separating the Responsible Protein Aggregates from the Innocent Bystanders. Annu Rev Neurosci. 2003; 26: 267–298. [PubMed: 12704221]

(2). Carulla N, Caddy GL, Hall DR, Zurdo J, Gairí M, Feliz M, Giralt E, Robinson CV, Dobson CM. Molecular Recycling Within Amyloid Fibrils. Nature. 2005; 436: 554–558. [PubMed: 16049488]

(3). Knowles TP, Fitzpatrick AW, Meehan S, Mott HR, Vendruscolo M, Dobson CM, Welland ME. Role of Intermolecular Forces in Defining Material Properties of Protein Nanofibrils. Science. 2007; 318: 1900–1903. [PubMed: 18096801]

(4). Ke PC, Sani M-C, Ding F, Kakinen A, Javed I, Separovic F, Davis TP, Mezzenga R. Implications of Peptide Assemblies in Amyloid Diseases. Chem Soc Rev. 2017; 46: 6492–6531. DOI: 10.1039/c7cs00372b [PubMed: 28702523]

(5). Nelson R, Sawaya MR, Balbirnie M, Madsen AO, Riekel C, Grothe R, Eisenberg D. Structure of the Cross-β Spine of Amyloid-Like Fibrils. Nature. 2005; 435: 773–778. DOI: 10.1038/nature03680 [PubMed: 15944695]

(6). Nyström G, Arcari M, Mezzenga R. Confinement-Induced Liquid Crystalline Transitions in Amyloid Fibril. Cholesteric Tactoids. Nat Nanotechnol. 2018; 13: 330–336. [PubMed: 29556006]

(7). Volpatti LR, Vendruscolo M, Dobson CM, Knowles TPJ. A Clear View of Polymorphism, Twist, and Chirality in Amyloid Fibril Formation. ACS Nano. 2013; 7: 10443–10448. [PubMed: 24359171]

(8). Liang C, Ni R, Smith JE, Childers WS, Mehta AK, Lynn DG. Kinetic Intermediates in Amyloid Assembly. J Am Chem Soc. 2014; 136: 15146–15149. [PubMed: 25313920]

(9). Knowles TPJ, Mezzenga R. Amyloid Fibrils as Building Blocks for Natural and Artificial Functional Materials. Adv Mater. 2016; 28: 6546–6561. [PubMed: 27165397]

(10). Knowles TP, Vendruscolo M, Dobson CM. The Amyloid State and its Association with Protein Misfolding Diseases. Nat Rev Mol Cell Biol. 2014; 15: 384–396. [PubMed: 24854788]

(11). Adler-Abramovich L, Vaks L, Carny O, Trudler D, Magno A, Caflisch A, Frenkel D, Gazit E. Phenylalanine Assembly into Toxic Fibrils Suggests Amyloid Etiology in Phenylketonuria. Nat Chem Biol. 2012; 8: 701–706. [PubMed: 22706200]

(12). Burdick D, Soreghan B, Kwon M, Kosmoski J, Knauer M, Henschen A, Yates J, Cotman C, Glabe C. Assembly and Aggregation Properties of Synthetic Alzheimers A4/Beta Amyloid Peptide Analogs. J Biol Chem. 1992; 267: 546–554. [PubMed: 1730616]

(13). Bernstein SL, Dupuis NF, Lazo ND, Wyttenbach T, Condron MM, Bitan G, Teplow DB, Shea J-E, Ruotolo BT, Robinson CV, Bowers MT. Amyloid-β Protein Oligomerization and the Importance of Tetramers and Dodecamers in the Aetiology of Alzheimer's Disease. Nat Chem. 2009; 1: 326–331. DOI: 10.1038/nchem.247 [PubMed: 20703363]

(14). Xu Y, Shen J, Luo X, Zhu W, Chen K, Ma J, Jiang H. Conformational Transition of Amyloid β-Peptide. Proc Natl Acad Sci U S A. 2005; 102: 5403–5407. DOI: 10.1073/pnas.0501218102 [PubMed: 15800039]

(15). Kusumoto Y, Lomakin A, Teplow DB, Benedek GB. Temperature Dependence of Amyloid Beta-Protein Fibrillization. Proc Natl Acad Sci U S A. 1998; 95: 12277–12282. DOI: 10.1073/pnas.95.21.12277 [PubMed: 9770477]

(16). Verel R, Tomka IT, Bertozzi C, Cadalbert R, Kammerer RA, Steinmetz MO, Meier BH. Polymorphism in an Amyloid-Like Fibril-Forming Model Peptide. Angew Chem, Angew Chem, Int Ed. 2008; 47: 5842–5845. [PubMed: 18528917]

(17). Schneider JP, Pochan DJ, Ozbas B, Rajagopal K, Pakstis L, Kretsinger J. Responsive Hydrogels from the Intramolecular Folding and Self-Assembly of a Designed Peptide. J Am Chem Soc. 2002; 124: 15030–15037. [PubMed: 12475347]

(18). Zimenkov Y, Dublin SN, Ni R, Tu RS, Breedveld V, Apkarian RP, Conticello VP. Rational Design of a Reversible pH-Responsive Switch for Peptide Self-Assembly. J Am Chem Soc. 2006; 128: 6770–6771. [PubMed: 16719440]

(19). Ozbas B, Kretsinger J, Rajagopal K, Schneider JP, Pochan DJ. Salt-Triggered Peptide Folding and Consequent SelfAssembly into Hydrogels with Tunable Modulus. Macromolecules. 2004; 37: 7331–7337.

(20). Wang F, Feng CL. Metal-Ion-Mediated Supramolecular Chirality of L-Phenylalanine Based Hydrogels. Angew Chem, Int Ed. 2018; 57: 5655–5659. [PubMed: 29571216]

(21). Ramadan D, Cline DJ, Bai S, Thorpe C, Schneider JP. Effects of As (III) Binding on β-Hairpin Structure. J Am Chem Soc. 2007; 129: 2981–2988. [PubMed: 17311379]

(22). Li J, Du XW, Hashim S, Shy A, Xu B. Aromatic-Aromatic Interactions Enable α-Helix to β-Sheet Transition of Peptides to Form Supramolecular Hydrogels. J Am Chem Soc. 2017; 139: 71–74. DOI: 10.1021/jacs.6b11512 [PubMed: 27997165]

(23). Li J, Zhan Z, Du X, Wang J, Hong B, Xu B. Selection of Secondary Structures of Heterotypic Supramolecular Peptide Assemblies by an Enzymatic Reaction. Angew Chem, Int Ed. 2018; 57: 11716–11721. DOI: 10.1002/anie.201806992 [PubMed: 29971927]

(24). Miller Y, Ma B, Nussinov R. Metal Binding Sites in Amyloid Oligomers: Complexes and Mechanisms. Coord Chem Rev. 2012; 256: 2245–2252.

(25). Hartgerink JD, Beniash E, Stupp SI. Self-Assembly and Mineralization of Peptide-Amphiphile Nanofibers. Science. 2001; 294: 1684–1688. [PubMed: 11721046]

(26). Hauser CAE, Zhang S. Designer Self-Assembling Peptide Nanofiber Biological Materials. Chem Soc Rev. 2010; 39: 2780–2790. [PubMed: 20520907]

(27). Wang M, Wang J, Zhou P, Deng J, Zhao Y, Sun Y, Yang W, Wang D, Li Z, Hu X, King SM, et al. Nanoribbons Self-Assembled from Short Peptides Demonstrate the Formation of Polar Zippers Between β-Sheets. Nat Commun. 2018; 9: 5118. doi: 10.1038/s41467-018-07583-2 [PubMed: 30504813]

(28). Yan XH, Zhu PL, Li JB. Self-Assembly and Application of Diphenylalanine-Based Nanostructures. Chem Soc Rev. 2010; 39: 1877–1890. [PubMed: 20502791]

(29). Cornwell DJ, Daubney OJ, Smith DK. Photopatterned Multidomain Gels: Multi-Component Self-Assembled Hydrogels Based on Partially Self-Sorting 1,3:2,4-Dibenzylidene-d-Sorbitol Derivatives. J Am Chem Soc. 2015; 137: 15486–15492. [PubMed: 26646708]

(30). Lampel A, Ulijn RV, Tuttle T. Guiding Principles for Peptide Nanotechnology through Directed Discovery. Chem Soc Rev. 2018; 47: 3737–3758. [PubMed: 29748676]

(31). Peters RJRW, Nijemeisland M, van Hest JCM. Reversibly Triggered Protein-Ligand Assemblies in Giant Vesicles. Angew Chem, Int Ed. 2015; 54: 9614–9617. [PubMed: 26089190]

(32). Che H, Cao S, van Hest JCM. Feedback-Induced Temporal Control of “Breathing” Polymersomes to Create Self-Adaptive Nanoreactors. J Am Chem Soc. 2018; 140: 5356–5359. DOI: 10.1021/jacs.8b02387 [PubMed: 29617118]

(33). Wang J, Liu K, Xing RR, Yan XH. Peptide Self-Assembly: Thermodynamics and Kinetics. Chem Soc Rev. 2016; 45: 5589–5604. [PubMed: 27487936]

(34). Rydzek G, Ji QM, Li M, Schaaf P, Hill JP, Boulmedais F, Ariga K. Electrochemical Nanoarchitectonics and Layer-by-Layer Assembly: From Basics to Future. Nano Today. 2015; 10: 138–167.

(35). Minami K, Kasuya Y, Yamazaki T, Ji Q, Nakanishi W, Hill JP, Sakai H, Ariga K. Highly Ordered 1D Fullerene Crystals for Concurrent Control of Macroscopic Cellular Orientation and Differentiation toward Large-Scale Tissue Engineering. Adv Mater. 2015; 27: 4020–4026. [PubMed: 26033774]

(36). Draper ER, Adams DJ. How Should Multicomponent Supramolecular Gels be Characterised? Chem Soc Rev. 2018; 47: 3395–3405. [PubMed: 29419826]

(37). Makam P, Gazit E. Minimalistic Peptide Supramolecular CoAssembly: Expanding the Conformational Space for Nanotechnology. Chem Soc Rev. 2018; 47: 3406–3420. DOI: 10.1039/c7cs00827a [PubMed: 29498728]

(38). Reches M, Gazit E. Casting Metal Nanowires within Discrete Self-Assembled Peptide Nanotubes. Science. 2003; 300: 625–627. [PubMed: 12714741]

(39). Goerbitz CH. The Structure of Nanotubes Formed by Diphenylalanine, The Core Recognition Motif of Alzheimer’s BetaAmyloid Polypeptide. Chem Commun. 2006. 2332–2334. [PubMed: 16733570]

(40). Reches M, Gazit E. Controlled Patterning of Aligned SelfAssembled Peptide Nanotubes. Nat Nanotechnol. 2006; 1: 195–200. [PubMed: 18654186]

(41). Hauser CAE, Maurer-Stroh S, Martins IC. AmyloidBased Nanosensors and Nanodevices. Chem Soc Rev. 2014; 43: 5326–5345. [PubMed: 24781248]

(42). Li Q, Jia Y, Dai L, Yang Y, Li J. Controlled Rod Nanostructured Assembly of Diphenylalanine and Their Optical Waveguide Properties. ACS Nano. 2015; 9: 2689–2695. [PubMed: 25759013]

(43). Li X, Fei J, Xu Y, Li D, Yuan T, Li G, Wang C, Li J. A Photoinduced Reversible Phase Transition in a Dipeptide Supra-molecular Assembly. Angew Chem, Int Ed. 2018; 57: 1903–1907. [PubMed: 29280315]

(44). Smith AM, Williams RJ, Tang C, Coppo P, Collins RF, Turner ML, Saiani A, Ulijn RV. Fmoc-Diphenylalanine Self Assembles to a Hydrogel via a Novel Architecture Based on π-π Interlocked β-Sheets. Adv Mater. 2008; 20: 37–41.

(45). Ramos Sasselli I, Halling PJ, Ulijn RV, Tuttle T. Supramolecular Fibers in Gels Can Be at Thermodynamic Equilibrium: A Simple Packing Model Reveals Preferential Fibril Formation versus Crystallization. ACS Nano. 2016; 10: 2661–2668. [PubMed: 26812130]

(46). Mahler A, Reches M, Rechter M, Cohen S, Gazit E. Rigid, Self-Assembled Hydrogel Composed of a Modified Aromatic Dipeptide. Adv Mater. 2006; 18: 1365–1370.

(47). Jacob R, Ghosh D, Singh PK, Basu SK, Jha NN, Das S, Sukul PK, Patil S, Sathaye S, Kumar A, Chowdhury A, et al. Self-Healing Hydrogels Composed of Amyloid Nano Fibrils for Cell Culture and Stem Cell Differentiation. Biomaterials. 2015; 54: 97–105. [PubMed: 25907043]

(48). Raeburn J, Mendoza-Cuenca C, Cattoz BN, Little MA, Terry AE, Zamith Cardoso A, Griffiths PC, Adams DJ. The Effect of Solvent Choice on the Gelation and Final Hydrogel Properties of Fmoc-Diphenylalanine. Soft Matter. 2015; 11: 927–935. [PubMed: 25516486]

(49). Raymond DM, Nilsson BL. Multicomponent Peptide Assemblies. Chem Soc Rev. 2018; 47: 3659–3720. DOI: 10.1039/c8cs00115d [PubMed: 29697126]

(50). Hamley IW. Small Bioactive Peptides for Biomaterials Design and Therapeutics. Chem Rev. 2017; 117: 14015–14041. [PubMed: 29227635]

(51). Chakraborty P, Bairi P, Roy B, Nandi AK. Improved Mechanical and Electronic Properties of Co-Assembled Folic Acid Gel with Aniline and Polyaniline. ACS Appl Mater Interfaces. 2014; 6: 3615–3622. [PubMed: 24495072]

(52). Ji W, Zhang S, Yukawa S, Onomura S, Sasaki T, Miyazawa K, Zhang Y. Regulating Higher-Order Organization through the Synergy of Two Self-Sorted Assemblies. Angew Chem, Int Ed. 2018; 57: 3636–3640. [PubMed: 29411922]

(53). Chin D-H, Woody RW, Rohl CA, Baldwin RL. Circular Dichroism Spectra of Short, Fixed-Nucleus Alanine Helices. Proc Natl Acad Sci U S A. 2002; 99: 15416–15421. DOI: 10.1073/pnas.232591399 [PubMed: 12427967]

(54). Shepherd NE, Hoang HN, Abbenante G, Fairlie DP. Single Turn Peptide Alpha Helices with Exceptional Stability in Water. J Am Chem Soc. 2005; 127: 2974–2983. [PubMed: 15740134]

(55). Mondal S, Adler-Abramovich L, Lampel A, Bram Y, Lipstman S, Gazit E. Formation of Functional Super-Helical Assemblies by Constrained Single Heptad Repeat. Nat Commun. 2015; 6: 8615. doi: 10.1038/ncomms9615 [PubMed: 26468599]

(56). Lara C, Gourdin-Bertin S, Adamcik J, Bolisetty S, Mezzenga R. Self-Assembly of Ovalbumin into Amyloid and Non-Amyloid Fibrils. Biomacromolecules. 2012; 13: 4213–4221. [PubMed: 23098330]

(57). Seo J, Hoffmann W, Warnke S, Huang X, Gewinner S, Schollkopf W, Bowers MT, von Helden G, Pagel K. An Infrared Spectroscopy Approach to Follow Beta-Sheet Formation in Peptide Amyloid Assemblies. Nat Chem. 2017; 9: 39–44. [PubMed: 27995915]

(58). Dong WK, Akogun SF, Zhang Y, Sun YX, Dong XY. A Reversible “Turn-On” Fluorescent Sensor for Selective Detection of Zn^{2+} Sens Actuators, B. 2017; 238: 723–734.

(59). Bolisetty S, Mezzenga R. Amyloid-Carbon Hybrid Membranes for Universal Water Purification. Nat Nanotechnol. 2016; 11: 365–371. [PubMed: 26809058]

(60). Peydayesh M, Bolisetty S, Mohammadi T, Mezzenga R. Assessing the Binding Performance of Amyloid-Carbon Membranes toward Heavy Metal Ions. Langmuir. 2019; 35: 4161–4170. [PubMed: 30811203]

(61). Zhou W, Saran R, Liu J. Metal Sensing by DNA. Chem Rev. 2017; 117: 8272–8325. [PubMed: 28598605]

(62). Peralta, J, Ogliaro, F, Bearpark, M, Heyd, J, Brothers, E, Kudin, K, Staroverov, V, Kobayashi, R, Normand, J, Raghavachari, K. Revision D 01. Gaussian, Inc; Wallingford, CT: 2013.

(63). Dreuw A, Weisman JL, Head-Gordon M. Long-Range Charge-Transfer Excited States in Time-Dependent Density Functional Theory Require Non-Local Exchange. J Chem Phys. 2003; 119: 2943–2946.

(64). Chiodo S, Russo N, Sicilia E. LANL2DZ Basis Sets Recontracted in the Framework of Density Functional Theory. J Chem Phys. 2006; 125: 104107. [PubMed: 16999515]

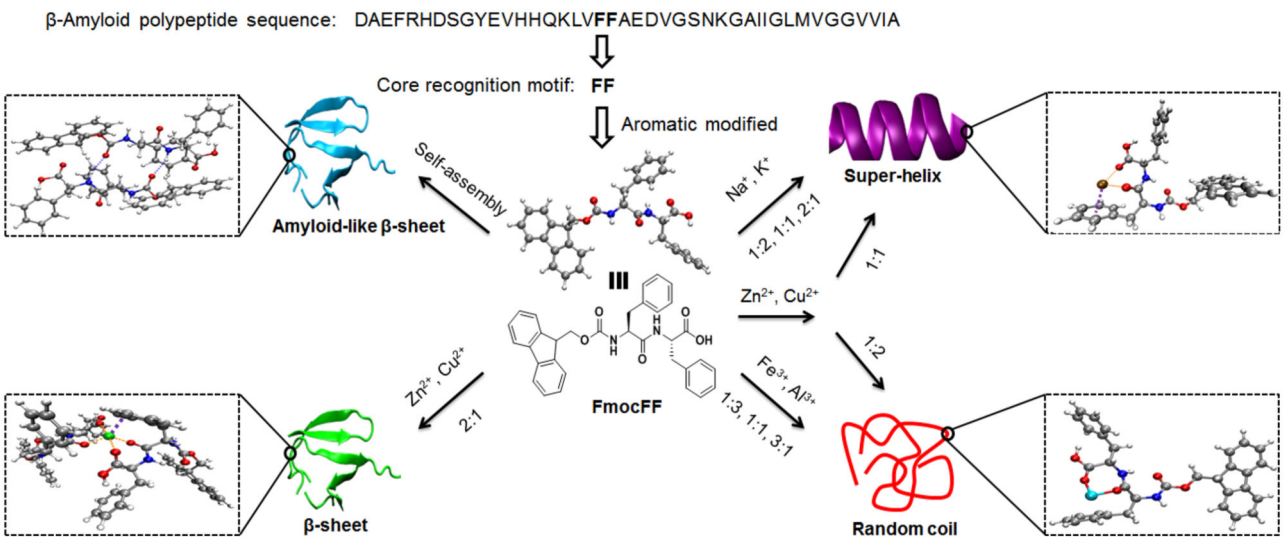

Figure 1. Schematic illustration of the metal-ion modulated structural transformation of amyloid-derived self-assembled FmocFF from the *β*-sheet into the superhelix and random coil. The molar ratios mentioned in the scheme are of FmocFF to metal ions. The coordination of metal ion with FmocFF is from DFT calculations.

Europe PMC Funders Author Manuscripts

Europe PMC Funders Author Manuscripts

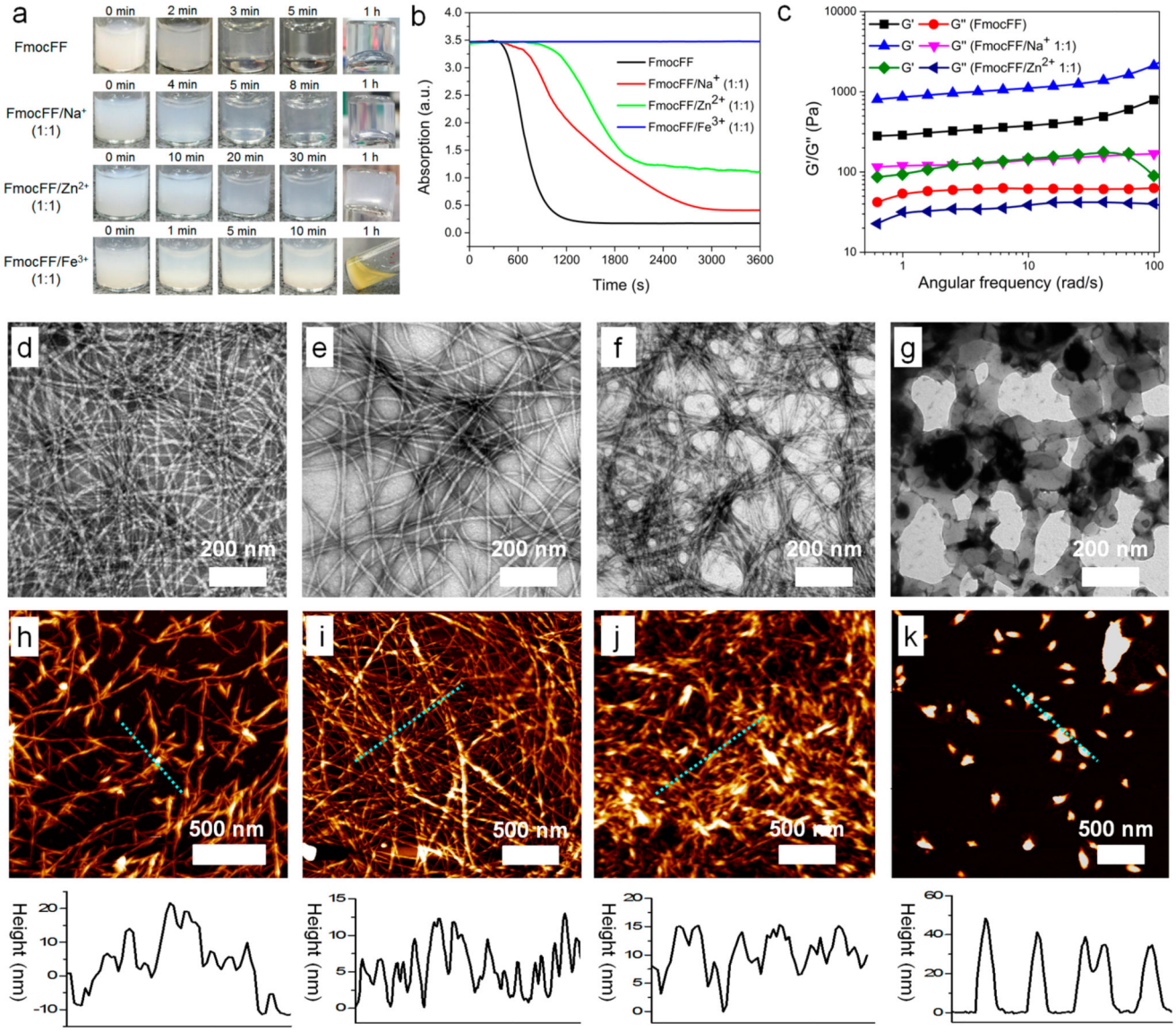

Figure 2.

(a) Time lapse optical images of FmocFF, FmocFF/Na^+ (1:1), FmocFF/Zn^{2+} (1:1), and FmocFF/Fe^{3+} (1:1) in 2% DMSO in H_2O (v/v) at a concentration of 2 mg/mL. 0 min represents the starting point after addition of FmocFF into the different metal ion soultions. (b) Turbidity measured at 405 nm over 3600 s for FmocFF, FmocFF/Na^+ (1:1), FmocFF/Zn^{2+} (1:1), and FmocFF/Fe^{3+} (1:1) solutions in 2% DMSO in H_2O (v/v). (c) Dynamic frequency sweep of gels of FmocFF, FmocFF/Na^+ (1:1), and FmocFF/Zn^{2+} (1:1) at a strain of 0.1% over a range of 0.1–100 $rads^{-1}$. (d–g) TEM images of (d) FmocFF, (e) FmocFF/Na^+ (1:1), (f) FmocFF/Zn^{2+} (1:1), and (g) FmocFF/Fe^{3+} (1:1) in 2% DMSO in H_2O (v/v). Scale bar is 200 nm. (h–k) AFM images (top) and height distribution (bottom) of (h) FmocFF, (i) FmocFF/Na^+ (1:1), (j) FmocFF/Zn^{2+} (1:1), and (k) FmocFF/Fe^{3+} (1:1) in 2% DMSO in H_2O (v/v). Scale bar is 500 nm.

Europe PMC Funders Author Manuscripts

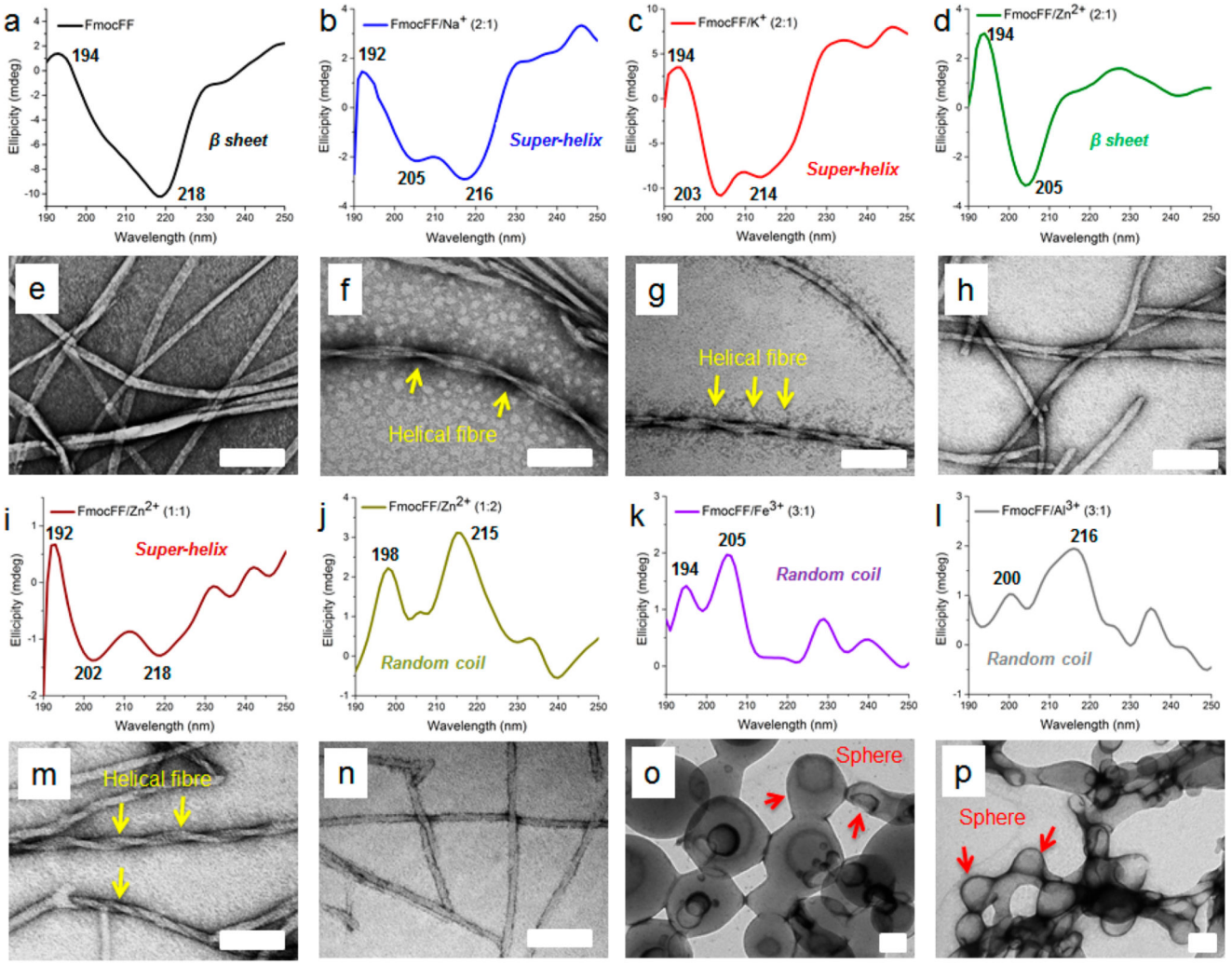

Figure 3.

(a–d, i–l) CD spectra and (e–h, m–p) high-resolution TEM images of FmocFF with different metal ions in 2% DMSO in H_2O (v/v) at a concentration of 2 mg/mL. (a, e) FmocFF, (b, f) FmocFF/Na^+ (2:1), (c, g) FmocFF/K^+ (2:1), (d, h) FmocFF/Zn^{2+} (2:1), (i, m) FmocFF/Zn^{2+} (1:1), (j, n) FmocFF/Zn^{2+} (1:2), (k, o) FmocFF/Fe^{3+} (3:1), and (l, p) FmocFF/Al^{3+} (3:1). Scale bar is 50 nm.

Europe PMC Funders Author Manuscripts

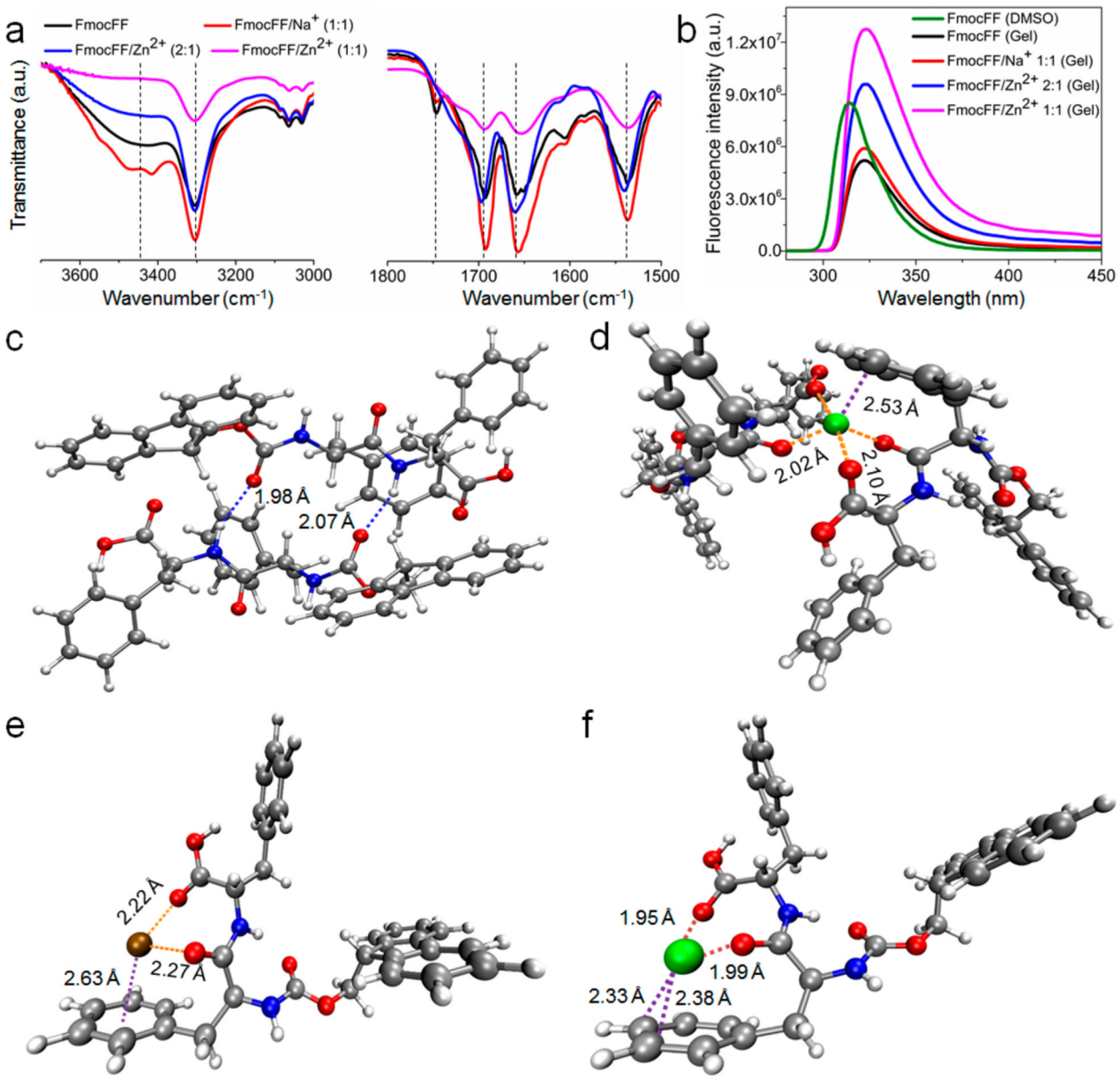

Figure 4.

(a) FTIR spectra of gels formed by FmocFF, FmocFF/Na^+ (1:1), FmocFF/Zn^{2+} (2:1), and FmocFF/Zn^{2+} (1:1). (b) Fluorescence emission spectra of FmocFF (DMSO), and gels formed by FmocFF, FmocFF/Na^+ (1:1), FmocFF/Zn^{2+} (2:1), and FmocFF/Zn^{2+} (1:1) at an excitation wavelength of 260 nm. (c) Molecular clusters of FmocFF. (d-f) Optimized geometries of all the metal ion-containing models of (d) FmocFF/Zn^{2+} (2:1), (e) FmocFF/Na^+ (1:1), and (f) FmocFF/Zn^{2+} (1:1) obtained by DFT calculations.

Europe PMC Funders Author Manuscripts

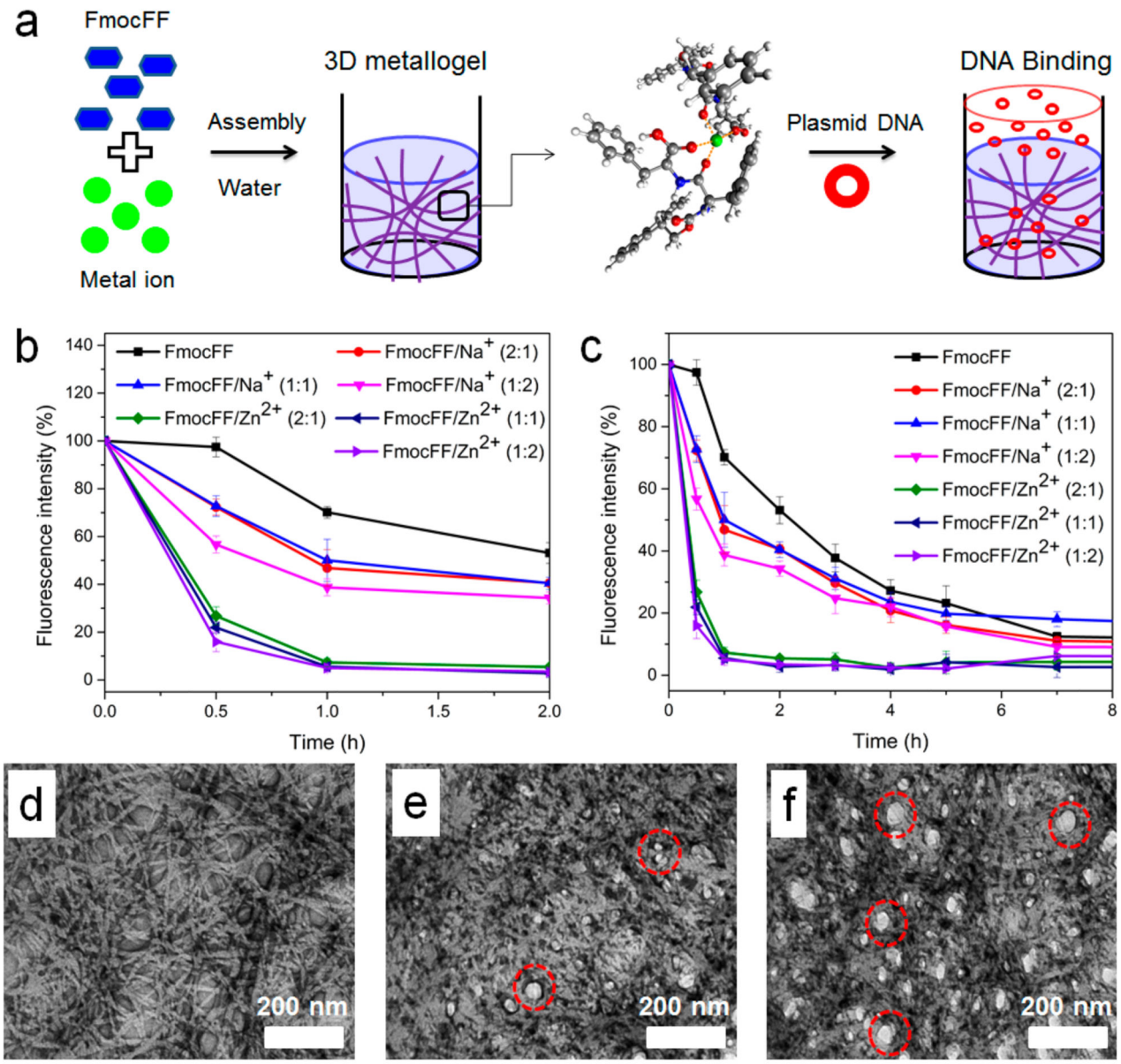

Figure 5.

(a) Schematic presentation of the preparation of 3D metallogels and their application in DNA binding. (b, c) Binding of DNA (syber safe assay) to gels formed by FmocFF, FmocFF/Na^+, and FmocFF/Zn^{2+} at different dipeptide/metal ion ratios via fluorescence measurements in short time of 2 h (b) and longtime of 8 h (c). (d–f) Time lapse TEM images of DNA binding to the FmocFF/Na^+ (1:1) hydrogel after addition of DNA: (d) 0 h, (e) 2 h, (f) 7 h. Scale bar is 200 nm.